UNIVERSITY OF CALIFORNIA
RIVERSIDE

Schottky Barrier Heights at Two-Dimensional Metallic and Semiconducting Transition-Metal Dichalcogenide Interfaces

A Thesis submitted in partial satisfaction
of the requirements for the degree of

Master of Science

in

Electrical Engineering

by

Adiba Zahin

December 2017

Thesis Committee:

Dr. Roger K. Lake, Chairperson
Dr. Alexander A. Balandin
Dr. Jianlin Liu

The Thesis of Adiba Zahin is approved:

Committee Chairperson

University of California, Riverside

Acknowledgments

This work was supported by FAME, one of the six centers of STARnet, a Semiconductor Research Corporation program sponsored by MARCO and DARPA and the NSF EFRI-1433395. This work used the Extreme Science and Engineering Discovery Environment (XSEDE), which is supported by the National Science Foundation Grant Nos. ACI-1053575 and ACI-1548562.

ABSTRACT OF THE DISSERTATION

Schottky Barrier Heights at Two-Dimensional Metallic and Semiconducting Transition-Metal Dichalcogenide Interfaces

by

Adiba Zahin

Master of Science, Graduate Program in Electrical Engineering
University of California, Riverside, December 2017
Dr. Roger K. Lake, Chairperson

Several advances have been made in the realization of electronic devices that utilize atomically thin two-dimensional (2D) materials. The semiconducting transition metal dichalcogenides in particular have been used to demonstrate a wide range of devices which include steep tunnel-field-effect transistors [1–6], photodetectors [7–12], field-effect-transistors [13–26] and chemical sensors [25, 27]. A variety of experimental [23, 28–37] and theoretical [38–43] studies have been devoted to understand the interface formed between the bulk metals that are deposited on the surface of the 2D transition metal dichalcognides. There is growing evidence that the Schottky-like transport behavior observed in TMDC-metal contacts is a consequence of strong Fermi level pinning (FLP). The origin of the Fermi level pinning in metal-TMDC interfaces has been attributed to the formation of interface dipoles [41, 44], defects at the metal-TMDC interface and the existence of metal-induced-gap-states (MIGS) which arise from the exponential decay of the wavefunction of the metal Fermi level into the TMDC band gap [45,46]. One approach to minimize the effect of Fermi level pinning would be achieving an epitaxially clean interface between the metal and the semiconducting TMDC. Prior experimental studies of the contact resistance between the 2H/1T polytypes of

MoS_2 succeeded in demonstrating record low contact resistance [47]. A recent study shows that FLP is weak for the metal-semiconductor junction (MSJ) formed by van der Waals (vdW) interactions, which is attributed to the suppression of MIGS in the semiconductor [48]. All 2D contacts may allow the tuning of the Schottky Barrier (SB) height (ϕ) by using different 2D metals.

To address this we investigate the use of 2D metallic TMDs (MX_2; M=Ta, Nb; X= S, Se,Te) as metal contacts instead of noble metals (Au, Pd, Ti, In etc) to 2D semiconducting TMDs (MX_2; M=Mo, W; X= S, Se,Te). We carry out a systematic study of the barrier heights and energy band lineups of the 2D semiconducting TMDs such as $MoSe_2$, WSe_2 and $MoTe_2$ with the 2D metallic TMDs such as NbS_2, $NbSe_2$, TaS_2 and $TaSe_2$ using ab initio density-functional theory (DFT) calculations. Using the calculated energy level alignments, we provide the values for the Schottky barrier heights for electron and hole injection for each combination of interfaces in vertical and lateral heterostructures.

Contents

List of Figures

List of Tables

Chapter 1

Introduction and Goals

1.1 Introduction

As the silicon microelectronics industry is rapidly approaching to the point where devices can no longer be scaled to progressively smaller size, an alternative material to silicon is needed for future logic transistor applications. The International Technology Roadmap for Semiconductors (ITRS) predicts that additional new materials and transistor geometries will be needed to successfully address the formidable challenges of transistor scaling in the next 15 years [50–52]. Correspondingly, to sustain the compelling demand of lower power consumption with higher performance in electronic systems the quest for new materials is crucial. Graphene has attracted significant attention in the electronic materials community, but it lacks a band gap which makes it unsuitable for digital electronic applications [53, 54]. Consequently several classes of two-dimensional (2D) compounds including boron nitride, metal chalcogenides, oxides, hydroxides, and oxychlorides have also received recent attention. A comprehensive list of all known layered van der Waals solids has been reported in a number of recent reviews [28, 55–59]. However, only a few of these layered materials can be classified as

semiconductors and even fewer have been successfully isolated as airstable, high-quality, two-dimensional crystals.

Transition metal dichalcogenides (TMDCs) are among the most studied layered compounds as atomically thin films of semiconducting TMDs have recently been isolated and characterized. The TMDC family exhibits a wide range of electrical properties depending on the polytypes and the number of transition metal d-electrons which include metallic [60–63], half-metallic [64], semiconducting [13, 61, 65, 66], superconducting [67] and charge density wave [63, 68–71] behavior. Monolayer 2D crystal semiconductors have extremely small thicknesses (few Å) and pristine interfaces without out-of-plane dangling bonds allows for FET application, this efficient electrostatics, reduces short channel effects and provides fewer traps on a semiconductor-dielectric interface.

1.1.1 Layered 2D Transition Metal Dichalcogenide

Transition metal dichalcogenides (TMDs) are composed of transition metal and chalcogen atoms. According to the International Union of Pure and Applied Chemistry (IUPAC) definition, transition metals are elements with a partially filled d sub-shell or which can give rise to cations with an incomplete d sub-shell specially from Group VIB through VIIB. Ti, Zr, Hf, Nb, Ta, Mo, W, Tc, and Re are all transition metal elements that occur in TMDs [28, 72, 73]. These materials have strong in-plane covalent or ionic bonding and weak out-of-plane van-der-Waal forces which enables exfoliation into two-dimensional layers of monolayer thickness with the help of advance exfoliation and synthetic techniques [74–77]. This weak interlayer coupling changes the properties of these materials as their thickness approaches the monolayer limit. Often, the bandgap changes from direct to indirect as it moves from monolayer to multi-layer. The layered materials form different kinds of stacking orders due to the weak interlayer forces. The

different stacking configurations such as $1T$, $2H_a$, $2H_b$, $2H_c$, $3R$, $4H_a$, $6R$ etc result in wide variety of electronic properties.

Experimental as well as theoretical studies shows that 2D layered materials have superior electronic, optical, mechanical and thermal properties than that of their bulk form [56, 58]. The self-passivated surfaces of these materials also makes it feasible to integrate heterostructures using different two dimensional materials and overcome limitations of dangling bonds associated with the growth and integration of unpassivated surfaces [78, 79].

1.1.2 Schottky Barrier

A Schottky barrier is a potential energy barrier for electrons formed at a metal-semiconductor junction (MSJ). Schottky barriers have rectifying characteristics, suitable for use as a diode. One of the primary characteristics of a Schottky barrier is the Schottky barrier height, denoted by Φ. The value of Φ depends on the metal and semiconductor surface state, dangling bonds, Fermi level pinning (FLP) etc. [80]. The energy barrier height has a significant impact on device performance for charge carrier transport across the MSJ [80, 81]. Φ is defined as the energy difference between the Fermi level (FL) and the semiconductor band edges in the junction

$$\Phi_e = E_{CBM} - E_F \tag{1.1}$$

$$\Phi_h = E_F - E_{VBM} \tag{1.2}$$

Here, Φ_e and Φ_h are the barrier heights for electrons and holes respectively, E_F is the Fermi energy and E_{VBM} and E_{CBM} are the energy of the valence band maximum (VBM) and conduction band minimum (CBM) of the semiconductor in the junction. Neglecting the metal-semiconductor interaction, Φ should ideally follow the predictions

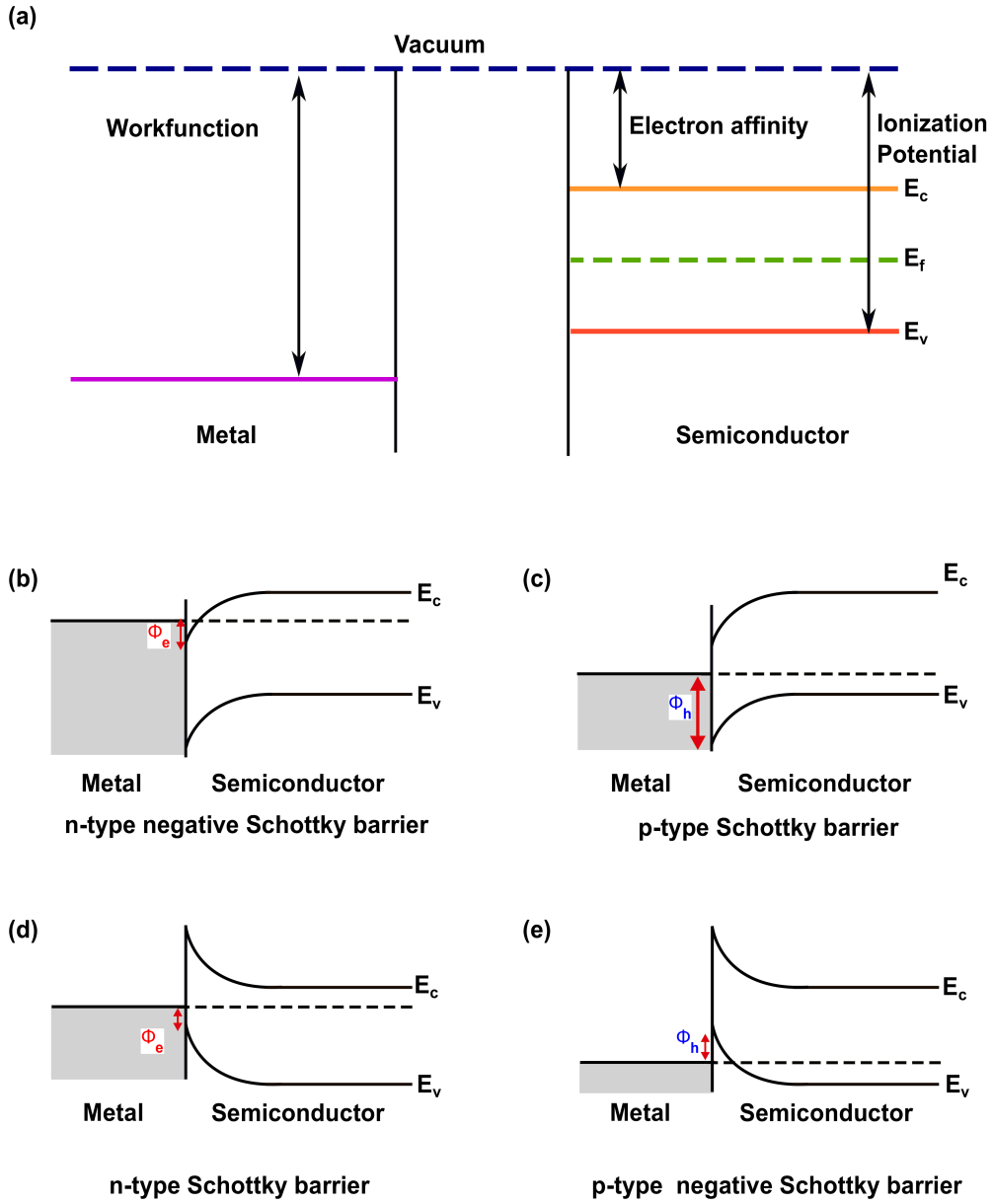

Figure 1.1: (a) Work function of metal; electron affinity and ionization potential of semiconductor. (b,d) are two possible n-type Schottky barriers (Φ_e); (c,e) are two possible p-type Schottky barriers (Φ_h).

of the Schottky-Mott model

$$\Phi_e = E_{ea} - W \tag{1.3}$$

$$\Phi_h = W - E_{ip} \tag{1.4}$$

where, W is the work function of the metal, and E_{ea} and E_{ip} are the electron affinity and ionization potential of the semiconductor in the junction. The work function of the metal, the electron affinity and the ionization potential of semiconductor are shown in Fig. 1.1(a). Fig. 1.1 also demonstrates the two possible n-type (b,d) and p-type (c,e) Schottky barrier heights.

1.2 Motivation and Goals

1.2.1 Contact Resistance

Experience shows that the access to a semiconductor region via a metal contact usually exhibits higher resistance than expected from an ideal contact. The additional resistance may be viewed as being a series resistor in the lead to the ideal contact. It shall be referred to as "contact resistance" [82]. If actual contact resistance is R_a and the ideal contact resistance is R_i then the contact resistance is then defined by the difference of these two resistances [82].

$$R_c = R_a - R_i \tag{1.5}$$

Contact resistance in the context of a metal/semiconductor heterostructure is the resistance contributed by the interface formed between the metal and semiconductor. In the case of a Schottky contact, the contact resistance is primarily contributed by thermionic and field emission over and across the Schottky barrier height and gives rise to rectifying behavior in current versus voltage. In an Ohmic contact in principle there is no barrier,

so the current versus voltage characteristics are linear and determined by the quality of the interface. This of course is an oversimplification and neglects several complications that can arise in experiments, eg. interface traps, roughness, etc

Contact resistance is a crucial determinant of FET performance. Low contact resistance in 2D semiconductor based devices is critical for achieving high on-state current, large photoresponse [7] and high-frequency operation [83]. Electrical metal contacts to two-dimensional (2D) semiconducting transition metal dichalcogenides (TMDCs) are found to be the key bottleneck to the realization of high device performance due to strong Fermi level pinning and the contact resistances (R_c) [84].

1.2.2 Fermi Level Pinning

Fermi level pinning refers to a situation where the band bending in a semiconductor contacting a metal is essentially independent of the metal even for large variation in the work function of the metal. A variety of experimental [23, 29, 85] and theoretical [41,42] studies have been devoted to understanding the interface formed between the bulk metals that are deposited on the surface of the 2D transition metal dichalcognides. There is growing evidence that the Schottky-like transport behavior observed in TMDC-metal contacts is a consequence of strong FLP. The origin of the FLP in metal-TMDC interfaces has been attributed to the formation of interface dipoles [41, 44], defects at the metal-TMDC interface and the existence of metal-induced-gap-states (MIGS) which arise from the exponential decay of the wavefunction of the metal Fermi level into the TMDC band gap [45, 46].

One approach to minimize the effect of Fermi level pinning would be achieving an epitaxially clean interface between the metal and the semiconducting TMDC [86]. High performance WSe_2 field effect transistors were demonstrated using van der Waals

assembly of substitutionally doped [26] and mixed-composition atomic layers between semiconducting and metallic TMDCs [87]. Experimental results show that $NbSe_2$ results in nearly ohmic p-type contacts to WSe_2 [88, 89]. $TaSe_2$ has also been demonstrated to be a low-resistivity contact to semiconducting TMDCs (s-TMDCs) ($MoSe_2$ and $HfSe_2$) [90]. An experimental and theoretical study identified and proposed Mo^{5+} rich interface region to have low hole Schottky barriers utilizing MoO_x contacts on MoS_2 and WSe_2 [91]. They suggest controlling the purity and stoichiometry of MoO_x will be key in realizing the potential of MoO_x as an efficient Ohmic hole injection contact. Experimental study have shown high performance, large-scale devices and circuits based graphene/MoS_2 heterostructure. They claim the tunability of the graphene work function with electrostatic doping significantly improves the ohmic contact to MoS_2 [92]. A very recent theoretical study also shows that the planar boron sheets (S1 and S2) are good candidates to form p-type Schottky contacts with the TMDCs ($MoSe_2$ and WSe_2) which can be tuned to a p-type ohmic contact upon an external electric field [93]. Prior experimental study have demonstrated record low contact resistance between the 2H/1T polytypes of MoS_2 [47]. They have demonstrated that the metallic 1T phase of MoS_2 can be locally induced on semiconducting 2H phase nanosheets, thus decreasing contact resistances to 200-300 μm at zero gate bias. They shoes the phase engineering can markedly reduce the contact resistance between the source/drain electrodes and the channel to enable high-performance FETs. Experimental study have also demonstrated true ohmic contact between 2H/1T$'$ phase of $MoTe_2$ [94]. These suggest that pristine metal TMDC interfaces offer a route to more transparent contacts.

1.2.3 Metallic Transition Metal Dichalcogenide

The Group V TMDCs are metallic in nature for all thicknesses from monolayer to bulk, and they exhibit the same self-passivated atomic structure as the Group VI TMDCs. An interface formed between a metallic and semiconducting TMDC would in principle be free of interface defects and this would lead to a reduction in the strength of the Fermi level pinning at the interface. A recent study shows that FLP is weak for the metal-semiconductor junction (MSJ) formed by van der Waals (vdW) interactions, which is attributed to the suppression of MIGS in the semiconductor [48]. It might allow the tuning of the Schottky Barrier (SB) height (ϕ) by using different 2D metals. They have predicted NbS_2 to be the most promising electrode with s-TMDCs [48].

Among the 2H family of transition metal dichalcogenides, NbS_2, $NbSe_2$, TaS_2, $TaSe_2$ are metallic in their nature [60, 61, 95]. Experimental study shows that, TaS_2 devices remained metallic despite the fabrication process [96]. Theoretical work shows that both monolayer NbX_2 and TaX_2 are metal. The NbS_2 sheet exhibits metallic behavior with one band crossing the Fermi level. The partial DOS analysis indicates this band is mainly attributed to the d orbitals of Nb atoms. Since the Nb (Ta) atom is one d electron less than the Mo (W) atom, the top d-character valence bands are not fully occupied and the metallicity appears in the monolayer NbX_2 (TaX_2) [97]. This result is consistent with the experimental observation that the TaS_2 films present robust metallic behaviors [96]. Thus, these monolayer metallic NbX_2 and TaX_2 would be one type of conducting materials for nano-devices [97].

Using a 2D metal as an electrode has other benefits. A 2D metal has limited electronic density of states (DOS) which gives low quantum capacitance. Thus, when charge is accumulated by applying a dielectric-mediated voltage, its work function (W)

changes markedly compared with conventional metals. This unique feature of a 2D metal leads to a gate-tunable W and therefore Schottky barrier (SB) height Φ, which have been observed in experiments [92,98–101]. The interface between the metal and the semiconductor is flat, which could facilitate carrier transport [86]. This atomically flat interface is difficult to achieve by using conventional metals. The suppression of MIGS reduces the electron-hole recombination at the interface, leading to a higher energy conversion efficiency for optoelectronic devices.

Chapter 2

Theoretical Methods

Density functional theory (DFT) is a computational quantum mechanical modeling method used to investigate the electronic structure of many-body systems particularly atoms, molecules and the condensed phases. DFT is among the most popular and versatile methods available in condensed-matter physics, computational physics and computational chemistry. DFT allows the many-electron Schrodinger equation to be solved in practice. The foundation of density functional theory are the Hohenberg-Kohn (HK) theorems [102]. The first HK theorem proves that the ground-state of a many-electron system is uniquely determined by the electron density of the system. The second HK theory states the total ground-state energy of such a many-electron system is a functional of the ground-state electron density. The Kohn-Sham approach [103] made the HK theorems computationally tractable. Within the framework of Kohn-Sham DFT (KS DFT), the many-body problem of interacting electrons in a static external potential is reduced to a problem of non-interacting electrons moving in an effective potential [103]. The effective potential includes the external potential and the effects of the Coulomb interactions between the electrons, e.g., the exchange and correlation in-

teractions. Basically, the Kohn-Sham approaches replaces the many-body electron wave function with a non-interacting system in an effective potential that has a ground state density that is identical to that of the many body interacting system. Two common approaches to approximate the exchange correlation potential include the local density approximation (LDA) and the generalized gradient approximation (GGA) [104, 105]. The main rationale behind these approximations is that for electron densities within a solid, exchange and correlation effects occur on a short length scale. Hence, LDA and GGA approximations of DFT accurately describe the properties of materials that resemble a homogeneous electron gas.

First-principles calculations of the TMDC heterostructures were carried out using DFT with a projector augmented wave method and the Perdew-Burke-Ernzerhof (PBE) type GGA [104,105] as implemented in the Vienna Ab Initio Simulation Package (VASP) [106]. A plane wave cutoff of 500 eV was used for all calculations. For each heterostructure the structural relaxation was performed until all forces were converged below 10 meV/Å. The workfunctions of the m-TMDs are determined using explicit slab calculations and the results are summarized in Fig. 3.1. For the slab calculations, a vacuum distance of 15 Å was used for each monolayer material. Then the difference between the electrostatic potential in the vacuum region and at the Fermi level gives us the workfunction (V_{vacuum} - E_F). Theoretical methods are covered in more detail in Chapter 3.3.1 and 3.4.1.

Chapter 3

Results and Discussions

3.1 Identifying the appropriate combination of the metal and semiconducting TMDC

Our investigations of the interface between the metal-semiconducting TMDCs first rely on identifying the appropriate combination of the metal and semiconducting TMDC which results in the lowest bi-axial, in-plane strain. Table 3.1 shows the lattice constant for the different materials investigated as part of this study and the calculated results are consistent with previous experimental and theoretical studies [97, 107–111]. The strain associated with the combination of the metallic and semiconducting TMDCs are shown in Table 3.1. We have relaxed each material to their ground state energy

Table 3.1: In-plane lattice constants, a_0, of the metallic & semiconducting TMDCs and the lattice mismatch associated with combinations of each material. Lattice mismatch values that are less than 2% have been highlighted in bold.

		$MoSe_2$	$MoTe_2$	WSe_2
a_0(Å)		3.31	3.53	3.34
a_0(Å)		Lattice mismatch (%)		
NbS_2	3.35	**1.21**	5.10	**0.30**
$NbSe_2$	3.47	4.83	**1.70**	3.89
TaS_2	3.35	**1.21**	5.10	**0.30**
$TaSe_2$	3.49	5.44	**1.13**	4.49

and have compared their lattice constants to find the lattice mismatch among them. We identify the combinations of semiconducting and metallic TMDCs that have a lattice mismatch lower than 5%. The metallic-TMDCs (m-TMDCs) occur in octahedral (1T) and trigonal-prismatic (2H) polytypes while the s-TMDCs have a trigonal prismatic (2H) coordination in their ground state. In our study we consider heterostructures with the m-TMDCs that have trigonal-prismatic coordination.

3.2 Band alignment of MX_2 and Workfunction of metal

The work functions of the m-TMDCs are in general larger than the work function of the noble metals that are conventionally used as contacts with the s-TMDCS [23,49]. We have calculated the workfunction of each 2D metallic TMDC (MX_2; M=Nb, Ta; X= S, Se) and align them with respect to vacuum other noble metals [23, 49] along with the calculated band alignment of 2D s-TMDCs ($MoSe_2$, $MoTe_2$,WSe_2), which is illustrated in Fig. 3.1. This large work function could be advantageous for good p-type contacts to the 2D semiconductors. Fig. 3.1, also shows the expected line-up of the m-TMDC Fermi levels with the bands of the s-TMDCs. All of the metallic TMDs are expected to have little to no barrier with the s-TMDC valence bands facilitating low-

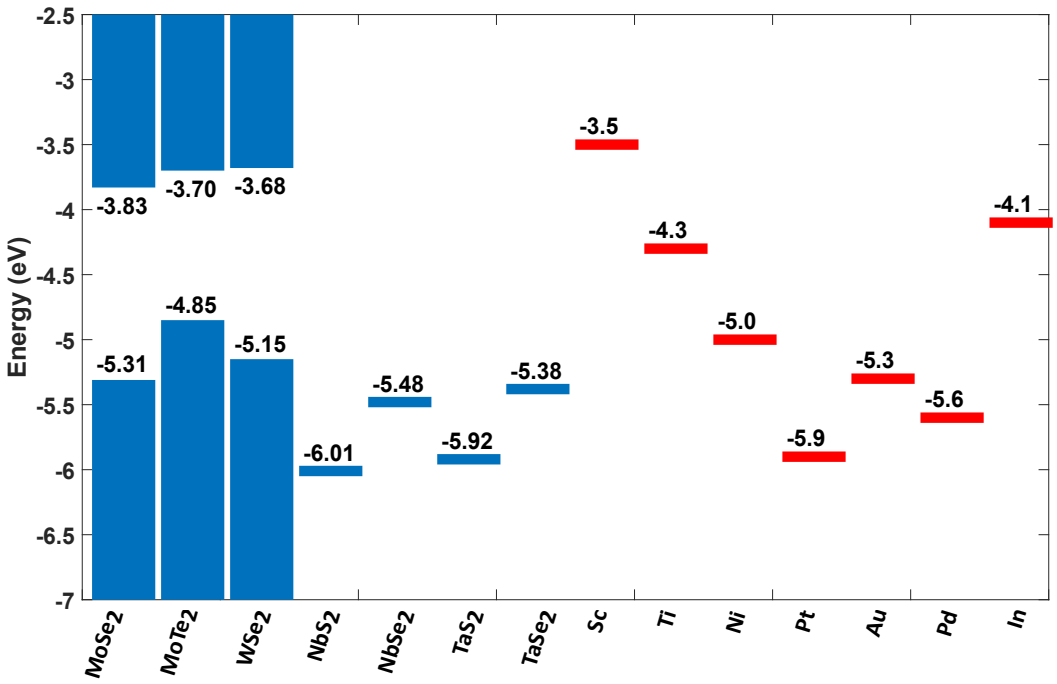

Figure 3.1: Calculated band alignment of MX_2 and work function of the metallic TMDCs along with the work function of noble metal from [23, 49]. The vacuum level is taken as zero reference.

resistance hole injection to the s-TMDCs. Graphically which can be represented by Fig. 3.2.

We have calculated the band alignments of these metal-semiconducting heterostructures using explicit interface calculations. For each heterostructure, the valence and conduction band offset is obtained by calculating the electronic band structure and identifying the band extrema contributed by the semiconducting and metallic TMDC.

3.3 Vertical Heterostructure

Fig. 3.3 demonstrates the vertical heterostructure with monolayer m-TMDC and monolayer s-TMDC. Fig. 3.3(a,b) are the side view and Fig. 3.3(c,d) are the top view of $2H_b$ and $2H_c$ stacking respectively. Here we have consider the following heterostructures: $MoSe_2$-NbS_2, $MoSe_2$-$NbSe_2$, $MoSe_2$-TaS_2, $MoTe_2$-$NbSe_2$, $MoTe_2$-$TaSe_2$,

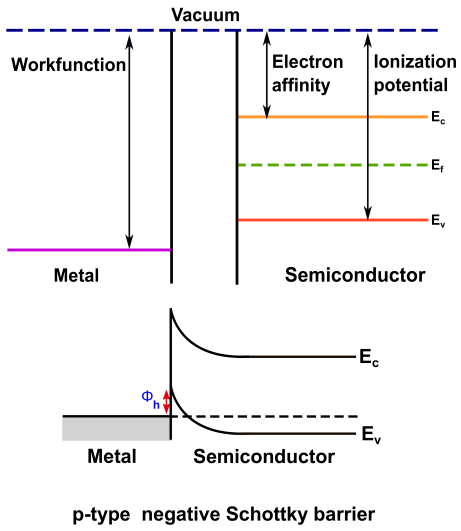

Figure 3.2: (a) Band diagram of metal and semiconductor with respect to vacuum, (b) possible band bending after contacting the metal and semiconductor.

WSe_2-NbS_2, WSe_2-$NbSe_2$ and WSe_2-TaS_2. We then calculate the band alignments of these metal-semiconducting heterostructures using explicit interface calculations.

3.3.1 Methodologies

In the vertical heterostructure to account the van-der-Waal interactions, the semiempirical Grimme-D2 [112] method was applied. We calculated the total energy verses lattice constant for each heterostructure and found the lowest energy structure to be the one in which the in-plane lattice constant of the heterostructure is the average of the two. Therefore, we used the average lattice constant of s-TMDCs and m-TMDCs. The lowest energy stacking polytype was used for each structure. The heterostructures are in the lowest energy for $2H_b$ stacking (Fig. 3.3(a,c)) with the exception of $MoTe_2$-$TaSe_2$, which has lowest energy in $2H_c$ stacking (Fig. 3.3(b,d)). A Monkhorst-Pack scheme [104] with 16×16×2 k-point grid was used for the structural relaxation and 8×8×1 k-point grid was used for self consistence field calculation.

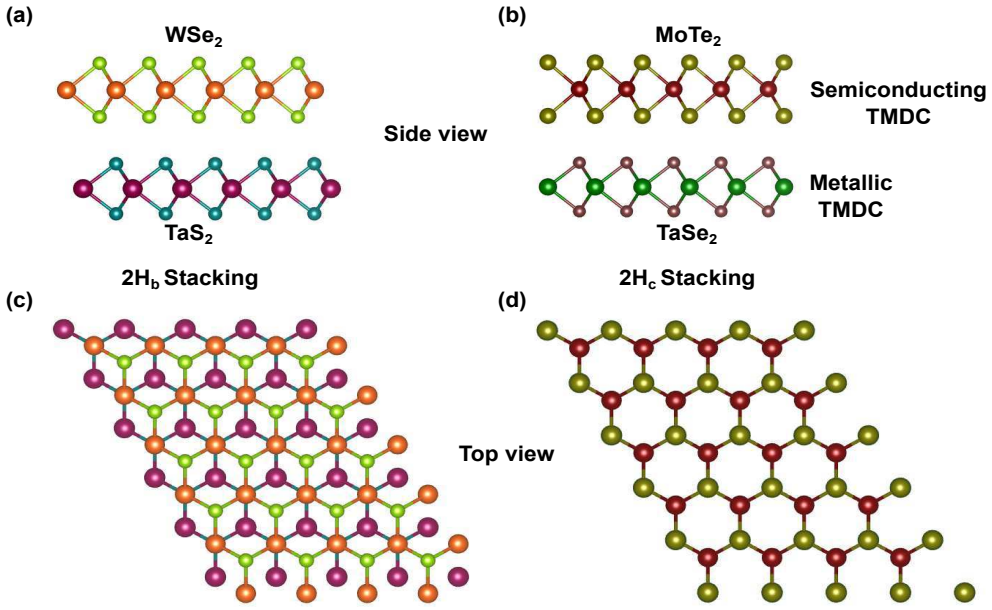

Figure 3.3: Vertical heterostructure with monolayer m-TMDC and monolayer s-TMDC. (a,b) are the side view and (c,d) are the top view of $2H_b$ and $2H_c$ stacking respectively.

3.3.2 Results

Fig. 3.4 shows the electronic band structure of all the metal-semiconductor heterostructures. Each k-point of each band is color coded according to its maximum orbital weight on each atom. All the materials along with their orbitals are color coded in Fig. 3.4. We have taken the Fermi energy as reference. The metal bands cross the Fermi energy. The closest band from s-TMDCs which lies below the Fermi level is the valence band and the closest band from s-TMDCs which lies above the Fermi level is the conduction band. The valence band offsets (VBO) are identified by calculating the energy difference between the s-TMDC valence band (d-orbital of Mo/W) and the Fermi energy. The VBO are shown with pink arrows. Similarly the conduction band offset (CBO) is identified by calculating the energy difference between the s-TMDC conduction band (d-orbital of Mo/W) and the Fermi energy. The green arrows of Fig. 3.4 represent the CBO. The valence band of the s-TMDCs in the heterostructure combination are $0.131 - 0.475$ eV below the Fermi level. The conduction band of the s-TMDCs in the

heterostructure combination are $0.762 - 1.318$ eV above the Fermi level.

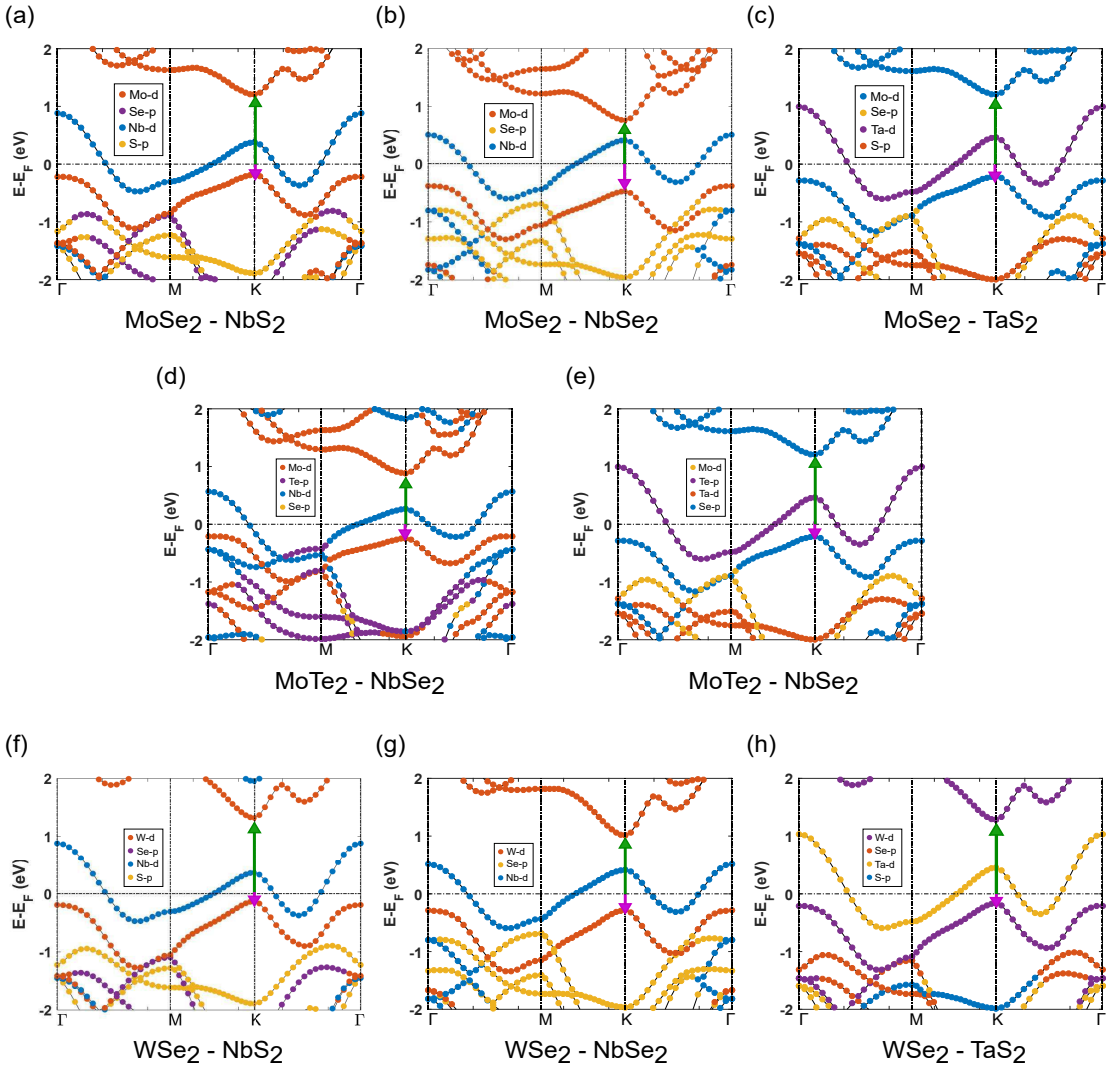

Figure 3.4: Electronic bandstructure of the metal-semiconductor heterostructures; (a)$MoSe_2$-NbS_2, (b)$MoSe_2$-$NbSe_2$, (c)$MoSe_2$-TaS_2, (d)$MoTe_2$-$NbSe_2$, (e)$MoTe_2$-$TaSe_2$, (f)WSe_2-NbS_2, (g)WSe_2-$NbSe_2$ and (h)WSe_2-TaS_2.

The VBO is significantly lower than the CBO. This trend occurs independent of the chalcogen or transition metal ion that constitutes the semiconducting or metallic TMDC. This can be understood by considering the alignment of the valence bands of the s-TMDCs and the m-TMDCs on an absolute scale as shown in Fig. 3.1. The large work function of the m-TMDCs leads to their Fermi level always near to the s-TMDCs

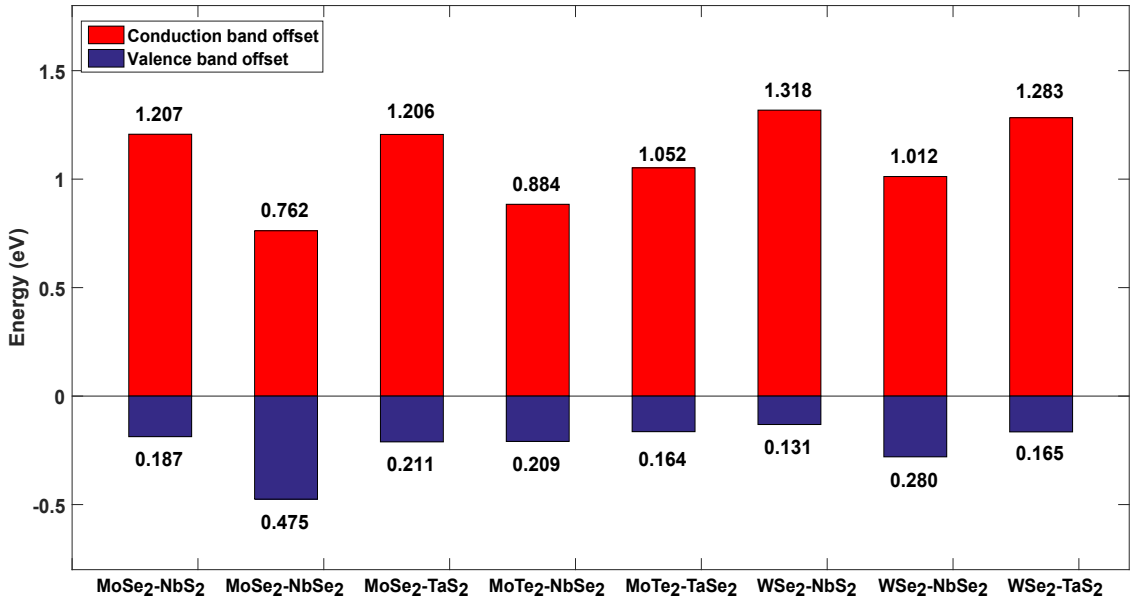

Figure 3.5: Conduction and Valance Band Offsets in the interface of monolayer Metal-monolayer Semiconductor heterostructure.

valence band.

Fig. 3.6(a,b,d,e) demonstrates, the charge density difference, $\Delta\rho$=ρ(metallic/ semiconducting TMDC)-ρ(m-TMDC)-ρ(s-TMDC) with their corresponding band structure. A surplus of electrons are shown in yellow near the m-TMDCs, and a deficiency of electrons are shown in blue near the s-TMDCs Fig. 3.6(a,d). The red color in Fig. 3.6(b,e) represents $\Delta\rho$ in the s-TMDC layer, and the blue color represents $\Delta\rho$ in the m-TMDC layer. The transfer of charge from the s-TMDC layer to the m-TMDC layer is consistent with the large work functions of the m-TMDCs shown in Fig. 3.1.

In conclusion, we have studied the band alignments between the semiconducting and metallic transition metal dichalcogenides from first principles. Our calculations highlight the ability to achieve interfaces with low valence band offsets between the semiconducting and metallic TMDCs. Such heterostructures could faciliate low resistance p-type contacts to monolayers semiconducting TMDCs.

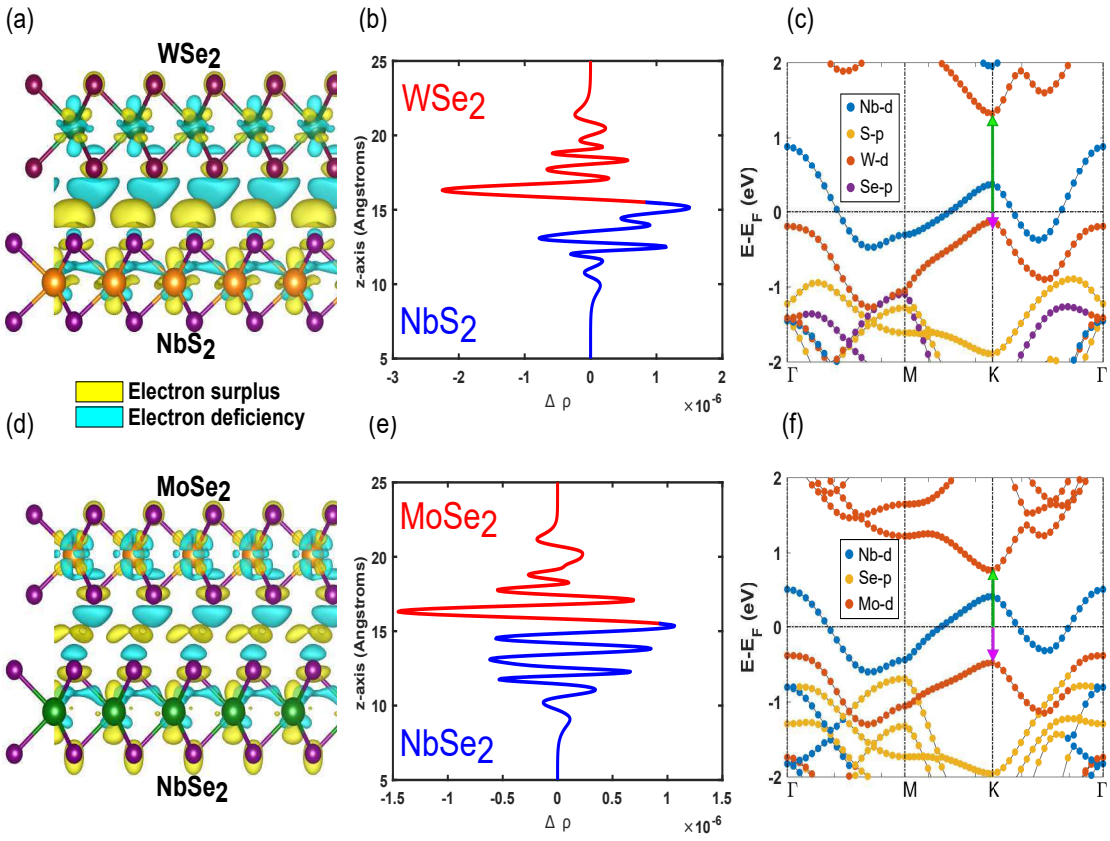

Figure 3.6: Charge transfer, charge density difference $\Delta\rho$, and electronic band structure at the interface of (a-c)WSe_2-NbS_2; (d-f)$MoSe_2$-$NbSe_2$ heterostructure.

3.4 Lateral Heterostructure

Lateral heterostructures have also been demonstrated in TMDCs [113, 114]. Therefore, we also consider lateral 2D metal-semiconductor heterostructures for all 2D contacts. We have studied the effects of interfaces formed between transition metal dichalcogenides by in-plane covalent bonds, with similar and dissimilar chalcogen atoms. Fig. 3.7(a) shows the lateral heterostructure of a monolayer m-TMDC and a monolayer s-TMDC formed by in-plane covalent bonds. Two type of interface geometries are considered, armchair and zigzag, as illustrated in Fig. 3.7(c,d). To create the armchair and zigzag interface, we start with the rectangular unit cell shown in Fig. 3.7(b) instead of the hexagonal primitive unit cell. We repeat the rectangular unit cell along the

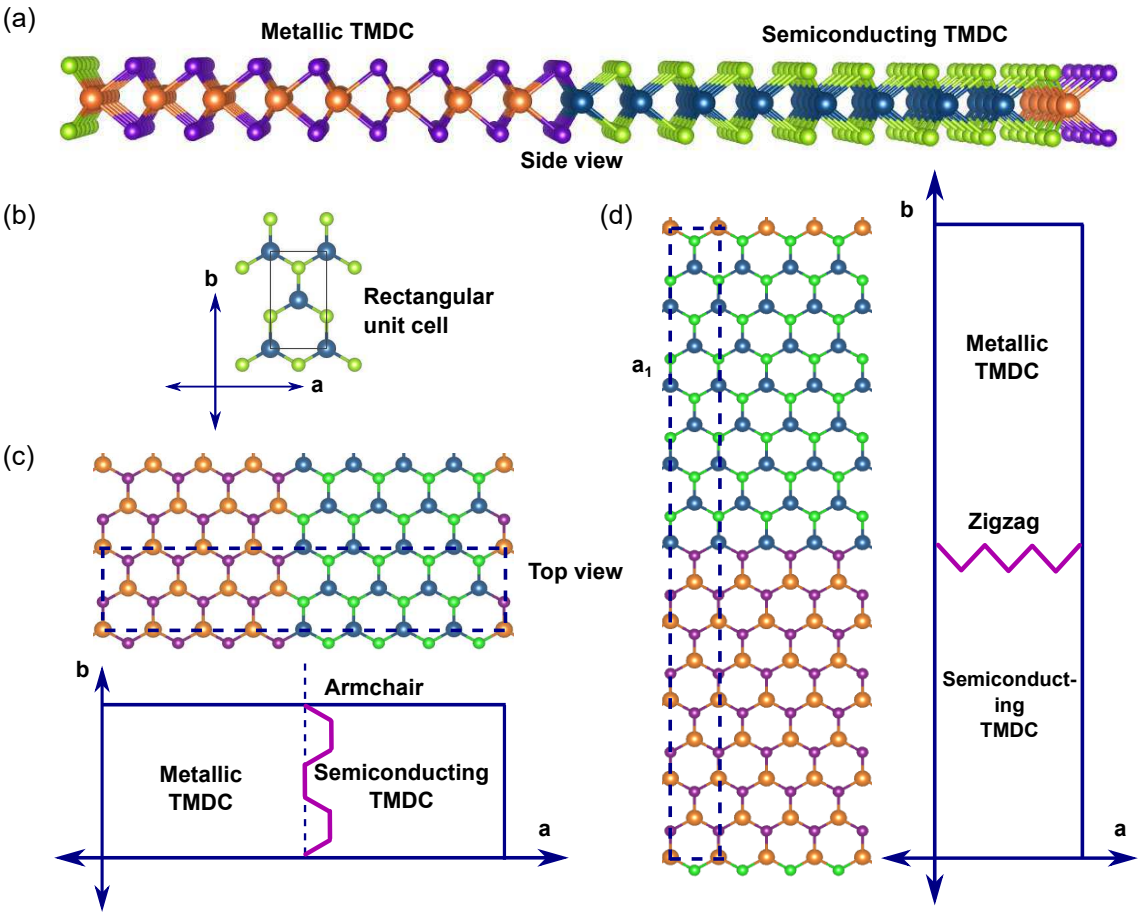

Figure 3.7: (a) Side view; top view of (c) an armchair interface and (d) a zigzag interface of lateral metal-semiconductor heterostructure. (b) Rectangular unit cell

a axis to obtain the armchair interface shown in Fig. 3.7(c), and we repeat it along the b axis to obtain the zigzag interface shown in Fig. 3.7(d). The dotted lines in Fig. 3.7(c,d) show the unit cell of each heterostructure configuration. The unit cell is periodic in all directions. We repeat the rectangular cell of Fig. 3.7(b) eight times to obtain four layers of metallic TMDCs and four layers of semiconducting TMDCs. The lattice vector a of the rectangular unit cell is smaller then the lattice vector b, so the armchair hetrostructure is smaller then the zigzag heterostructure.

Fig. 3.8 shows the rectangular Brillouin zone (BZ) in purple corresponding to the rectangular unit cell of Fig. 3.7(b) tiled over the hexagonal BZ of the hexagonal primitive unit cell in red. The K and $K^{'}$ points in the hexagonal BZ (H-BZ) are shown

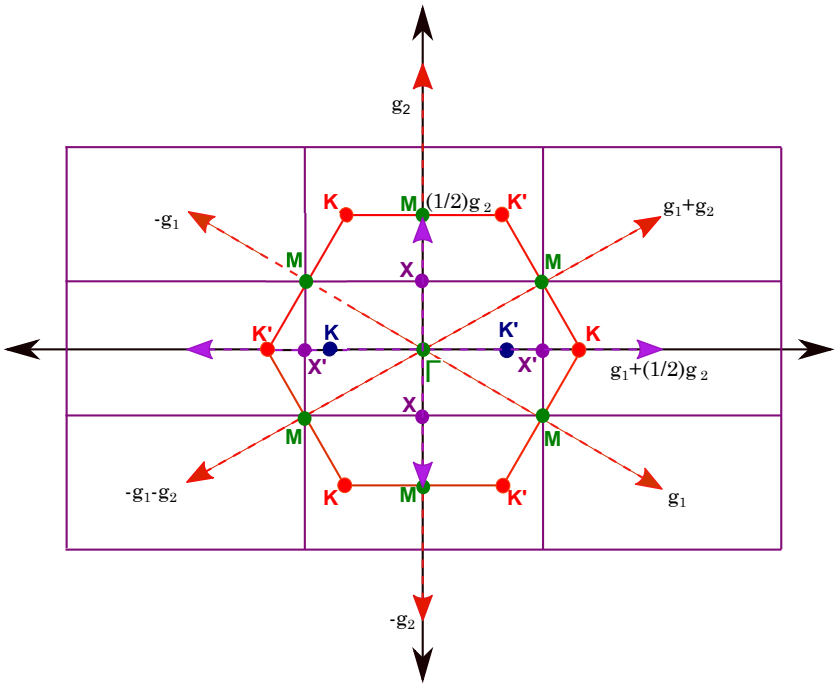

Figure 3.8: Hexagonal (red) and rectangular (purple) Brillouin zone (BZ). The K and $K^{'}$ points in the hexagonal BZ are shown in red. The $X^{'}$, X points in the rectangular BZ are shown in purple. The Γ and M points are the same in both hexagonal and rectangular BZ shown in green. The K and $K^{'}$ points maps back to rectangular BZ shown in blue.

in red. The $X^{'}$, X points in the rectangular BZ (R-BZ) are shown in purple. Four of the H-BZ M points map onto the corners of the R-BZ, and two of the H-BZ M points map back to Γ in the R-BZ. The K and $K^{'}$ points in the H-BZ lie in the extended zone of the R-BZ. This results in a mapping back of the the six K and $K^{'}$ points to the Γ–X' line in the R-BZ shown in blue. In Fig. 3.8, g_1 and g_2 are the reciprocal lattice constants of the H-BZ of $MoSe_2$. The reciprocal lattice constants of the R-BZ are $g_1^r = g_1 + \frac{1}{2}g_2$ and $g_2^r = \frac{1}{2}g_2$.

3.4.1 Methodologies

For each material system and each interface geometry, we considered two structures, one with the s-TMDC strained coherently to the m-TMDC and the other with m-TMDC strained coherently to the s-TMDC. For both, a complete internal relaxation

of all of the atomic coordinates was performed. A 1×6×1 Monkhorst-Pack scheme [104] was used for the armchair heterostructure and a 6×1×1 Monkhorst-Pack scheme was used for the zigzag heterostructure relaxation and self consistence field calculation. Two metal-semiconductor heterostructures are considered, $MoSe_2$-TaS_2 and WSe_2-$NbSe_2$.

3.4.2 Results

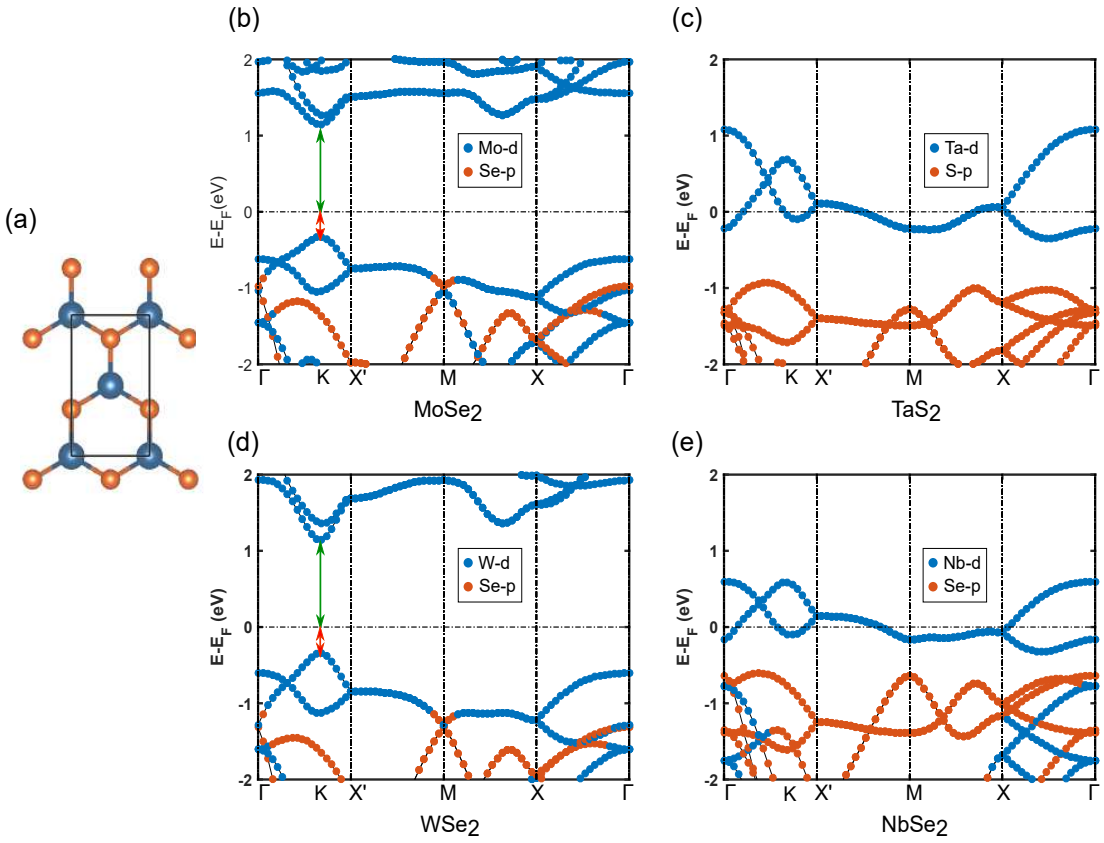

Figure 3.9: (a) Rectangular unit cell and the electronic band structure of molayer (b) $MoSe_2$, (c) TaS_2, (d) WSe_2 and (e) $NbSe_2$ rectangular unit cell.

Before investigating the heterostructures, we first plot the electronic bandstructure of the 4 different materials calculated using the rectangular unit cell of Fig.3.9(a). Fig. 3.9(b-e) are the electronic band structures of the rectangular unit cells of $MoSe_2$, TaS_2, WSe_2 and $NbSe_2$, respectively. The VBO and the CBO of the two s-TMDCs are

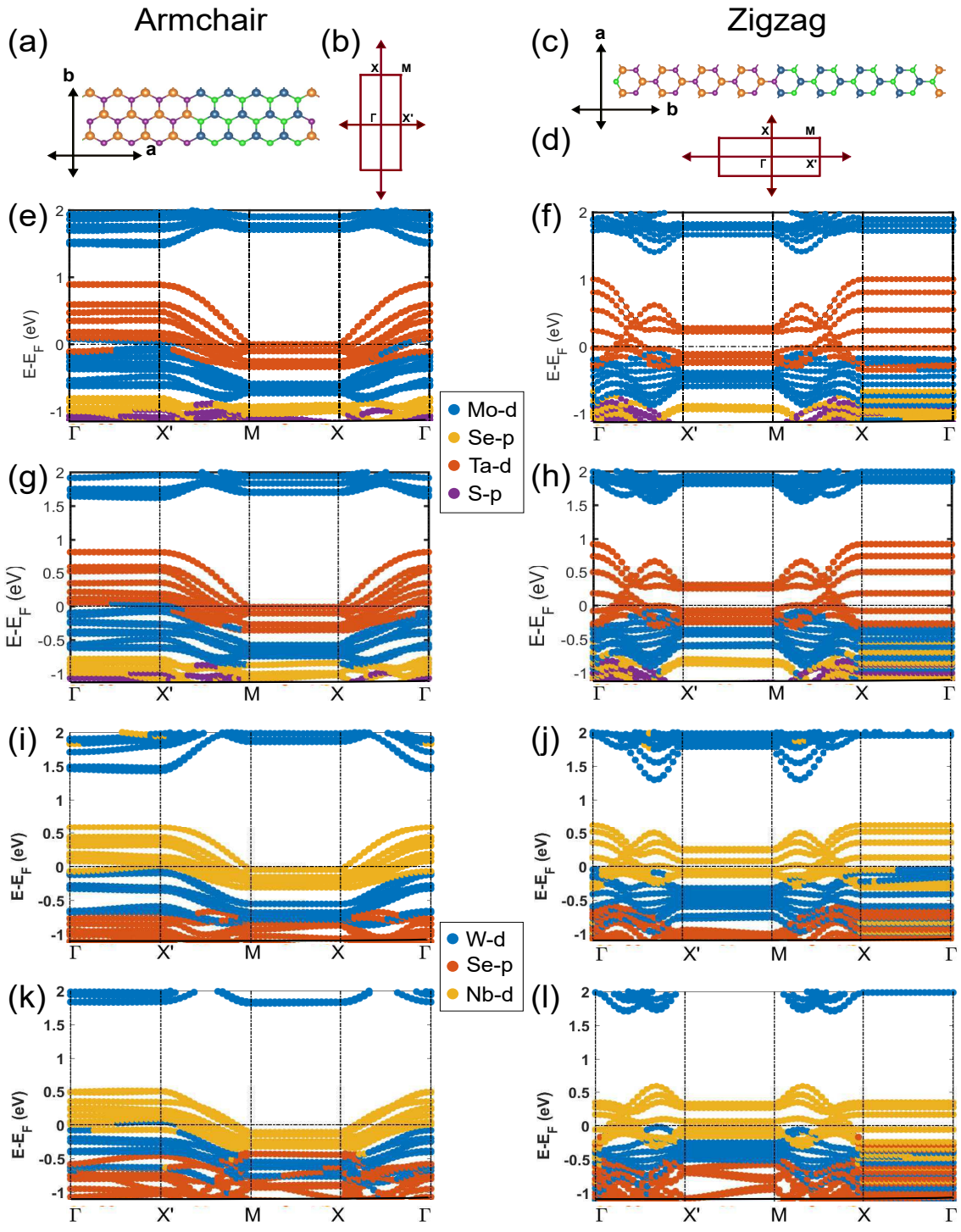

Figure 3.10: Atomistic supercells simulated for in-plane, monolayer heterojunctions with an armchair interface and a zigzag interface. (a) The rectangular unit cell of armchair interface and (b) the corresponding BZ. (c) The rectangular unit cell of zigzag interface and (d) the corresponding BZ. The corresponding E-k relation is shown under each supercell with the bands color coded to show the atom with the maximum projected density of states as given in the legends. (e,f) $MoSe_2$ is strained to match the lattice constant of TaS_2. (g,h) TaS_2 is strained to match the lattice constant of $MoSe_2$. (i,j) WSe_2 is strained to match the lattice constant of $NbSe_2$. (k,l) $NbSe_2$ is strained to match the lattice constant of WSe_2.

Table 3.2: VBO and CBO in the lateral heterostructure.

Heterostructure		$MoSe_2$-TaS_2		WSe_2-$NbSe_2$	
Interface		$MoSe_2$ is strained to match the lattice constant of TaS_2	TaS_2 is strained to match the lattice constant of $MoSe_2$	WSe_2 is strained to match the lattice constant of $NbSe_2$	$NbSe_2$ is strained to match the lattice constant of WSe_2
Armchair	k-path VBM k-path CBM	$\Gamma - X^{'}$ 0.08 $X^{'}$ 1.479	$\Gamma - X^{'}$ 0.042 $X^{'}$ 1.619	$X^{'}$ -0.068 $X^{'}$ 1.426	$X^{'}$ 0.0455 M 1.811
Zigzag	k-path VBM k-path CBM	$\Gamma - X^{'}$ -0.066 $\Gamma - X^{'}$ 1.410	$\Gamma - X^{'}$ -0.061 $\Gamma - X^{'}$ 1.550	Γ -0.047 $\Gamma - X^{'}$ 1.295	Γ -0.019 $\Gamma - X^{'}$ 1.708

shown with green and red arrows, respectively, and they occur along the Γ–X' line as discussed above.

The electronic band structure of the heterostructures are shown in Fig. 3.10. The heterostructure unit cells are shown in Fig. 3.10(a,c), and the corresponding electronic band structure for the two different material combinations and strain are shown below. The rectangular BZs corresponding to the heterostructure unit cells are shown in Fig. 3.10(b,d). From the electronic band structure in the Fig. 3.10(e-l), we extract the CBO and VBO formed at the interface of two lateral heterostructures each in two different strain conditions. Fig. 3.10(e,g) shows a band with primary contribution from the Mo atom of the $MoSe_2$-TaS_2 heterostructure lying at the Fermi level. This indicates that the valence band of $MoSe_2$ lies at the Fermi level of TaS_2 in this horizontal armchair heterojunction configuration providing a zero-barrier contact for holes. Similarly, the valence band of WSe_2 lies at the Fermi level of $NbSe_2$ in the armchair WSe_2-$NbSe_2$ heterostructure as shown Fig. 3.10(i,k). Table 3.2 shows all of the magnitudes and positions of the VBO and CBO of the lateral heterostructure.

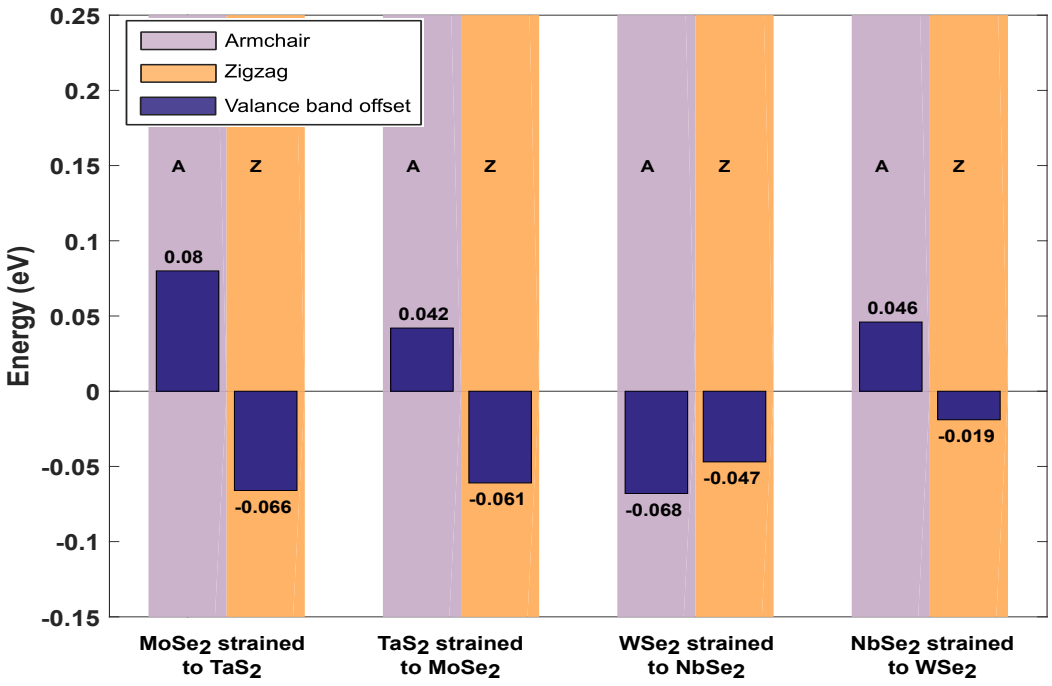

Figure 3.11: Valence band offsets of the lateral metal-semiconductor heterostructures.

The valence band offsets from the heterostructure calculations are shown in Fig. 3.11. In the zigzag heterojunction, the valence band of $MoSe_2$ in the $MoSe_2$-TaS_2 heterostructure is $\sim$ 60 meV below the Fermi level of TaS_2 for both strain configurations. The valence band of WSe_2 in the zigzag WSe_2-$NbSe_2$ heterostructure is 47 meV or 19 meV below the Fermi level of $NbSe_2$ as depending on the strain configuration.

The armchair heterostructures show negative Schottky barriers. The valence band of $MoSe_2$ is above the Fermi level for both strain configurations resulting in negative Schottky barriers. The barriers are 80 meV for $MoSe_2$ strained to TaS_2 and 42 meV for TaS_2 is strained to $MoSe_2$. The valence band of WSe_2 in the armchair WSe_2-$NbSe_2$ heterostructure is more sensitive to strain. Straining the WSe_2 to the $NbSe_2$ results in a positive Schottky barrier of 68 meV whereas straining the $NbSe_2$ to the WSe_2 gives a negative schottky barrier of 46 meV. Except for one strain configuration of the WSe_2-

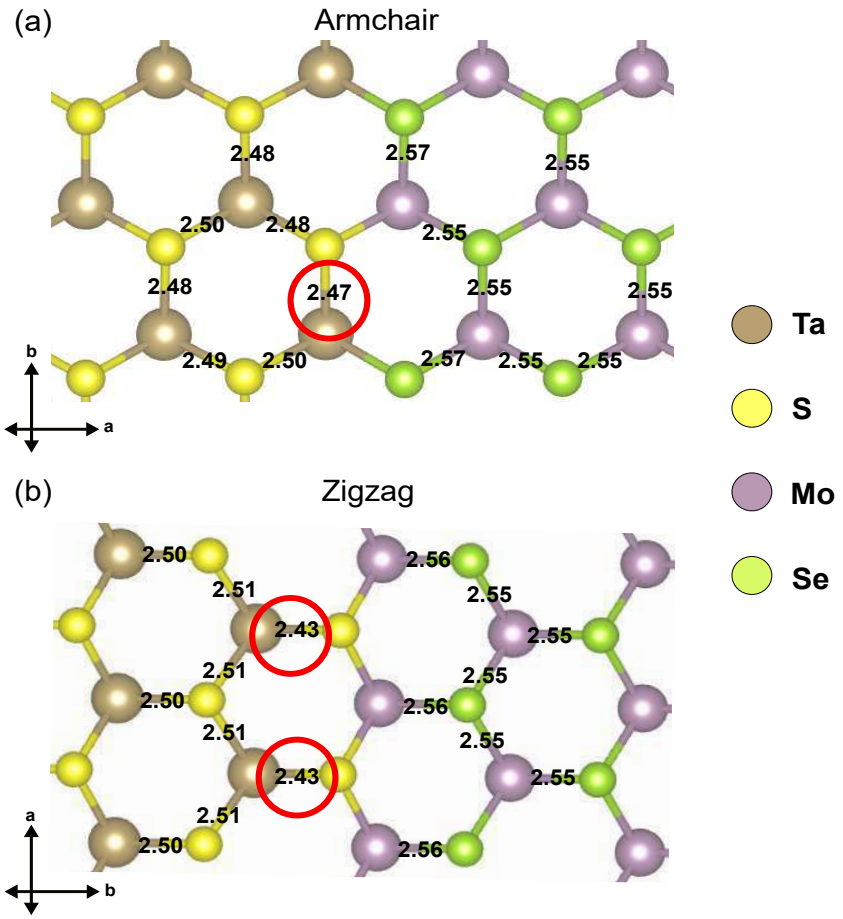

Figure 3.12: Bond lengths (in Å) of (a) armchair and (b) zigzag interface of $MoSe_2$-TaS_2 lateral heterostructures. The strained interface bonds are circled in red.

$NbSe_2$ heterostructure, the armchair interface results in a negative Schottky barrier contact. In all cases, the zigzag interface gives a positive Schottky barrier with the Fermi level above the valence band edge.

One reason for the different barrier hight for different interfaces could be the different strain associated with the armchair and zigzag interfaces. Fig. 3.12 shows the bond lengths of armchair and zigzag interfaces of the $MoSe_2$-TaS_2 heterostructures where $MoSe_2$ is strained to match the lattice constant of TaS_2. The initial bond lengths of Mo–Se and Ta–S were 2.48 Å, and after relaxation the Mo–Se bond lengths became $\sim$ 2.57 Å at the armchair interface and 2.56 Å at the zigzag interface and 2.55 Å away from the interface for both armchair and zigzag configuration. The bond lengths of Ta–S

became 2.47 Å at the interface and 2.48-2.50 Å away from the interface for armchair configuration. The bond lengths of Ta–S became 2.43 Å at the interface and 2.50-2.51 Å away from the interface for zigzag configuration. The Ta–S bond lengths are strained $\sim 0.4\%$ at the armchair interface and 2% at the zigzag interface. Thus, the strain in the interface Ta–S bonds is considerably higher at the zigzag interface than at the armchair interface. This difference in strain might be one mechanism that alters the energy level alignments.

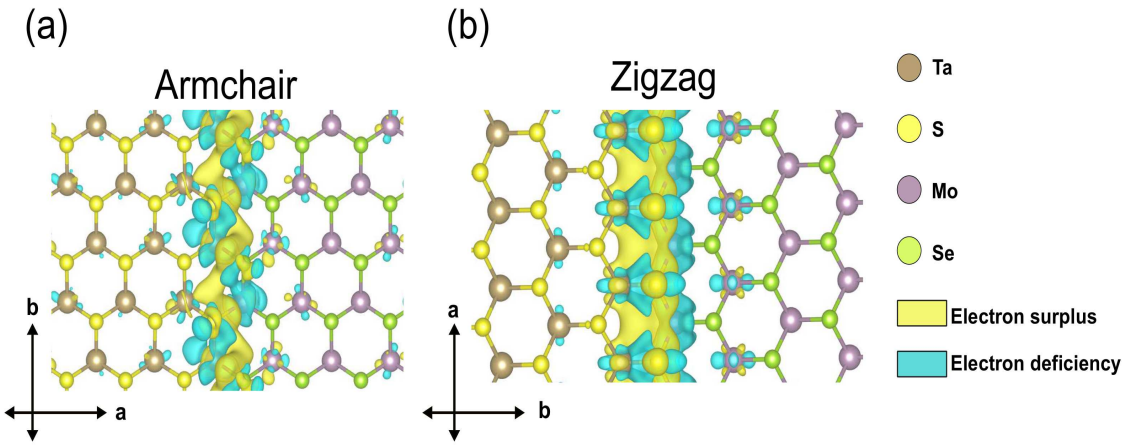

Figure 3.13: Charge transfer at the (a) armchair and (b) zigzag interface of $MoSe_2$-TaS_2 lateral heterostructures.

It is also known that the energy levels of the edge states of TMDCs depend on the type of edge. The energetics are similar to those of graphene edges. Passivated armchair edges of MoS_2 are semiconducting with a smaller gap than that of the the bulk, and zigzag edges are always metallic with an edge state crossing the Fermi level within the bulk bandgap [115]. This metallic edge state could either pin or shift the Fermi level

into the gap in a zizag interface. Understanding the physical mechanisms governing the edge dependence of the band alignment is still an open line of investigation.

Fig. 3.13 illustrates the charge transfer in the armchair and zigzag interface of $MoSe_2$-TaS_2 lateral heterostructures. Yellow indicates electron surplus and the blue indicates electron deficiency. This indicates there is a charge transfer between the metal and semiconducting TMDCs, but it's significance in terms of understanding the different offsets resulting from different interface is not clear.

Chapter 4

Conclusions

The electronic properties of the vertical and lateral metal-semiconductor TMDC heterostructure have been studied by first-principle calculations. To improve the contact resistance and to avoid FLP, we used m-TMDCs as contacts to s-TMDCs. In the $MoSe_2$-NbS_2, $MoTe_2$-$TaSe_2$, WSe_2-NbS_2, and WSe_2-TaS_2 vertical heterostructures, the VBM is less then 0.2 eV below the Fermi level. Our calculations highlight the ability to achieve interfaces with low valence band offsets between the semiconducting and metallic TMDCs. In the lateral metal-semiconductor TMDC heterostructures, the armchair $MoSe_2$-TaS_2 heterostructure in two strain condition and the armchair WSe_2-$NbSe_2$ heterostructure where the $NbSe_2$ is strained to WSe_2, have the VBM of the s-TMDCs lying above the Fermi level, creating a negative p-type Schottky barrier A negative p-type Schottky barrier is desired for low resistance hole injection. Our calculations predict that the metal-semiconducting TMDCs vertical and lateral heterostructure could facilitate low-resistance p-type contacts with pristine interfaces to monolayer TMCDs.

Chapter 5

Future Plan

In the horizontal heterostructures, the potential in the direction perpendicular to the interfaces is that of a superlattice, since periodic boundary conditions are applied to the supercells. If the semiconducting regions are short enough, the metal states can tunnel through the semiconducting region and couple to the next metal region in the adjacent unit cells. When this happens, superlattice minibands form, and the energetic width of the miniband gives the strength of the coupling. The formation of minibands results in energy broadening of the metal states, and if this energy broadening is similar to the Fermi level alignment, then it puts the value of the alignment energy into question. If we zoom in to the $\Gamma - X^{'}$ path of the armchair configuration of $MoSe_2$-TaS_2, there is some dispersion to the bands as shown in Fig. 5.1(b). There are cosine minibands near the Fermi level with bandwidth of 50 meV. These bandwidths are of the same order as the band offsets. The energy broadening due to the mini bands may effect the calculated band offsets.

To clarify this, we will to eliminate the coupling through the semiconducting region by increasing the length of the semiconductor region. We will simulate the lateral

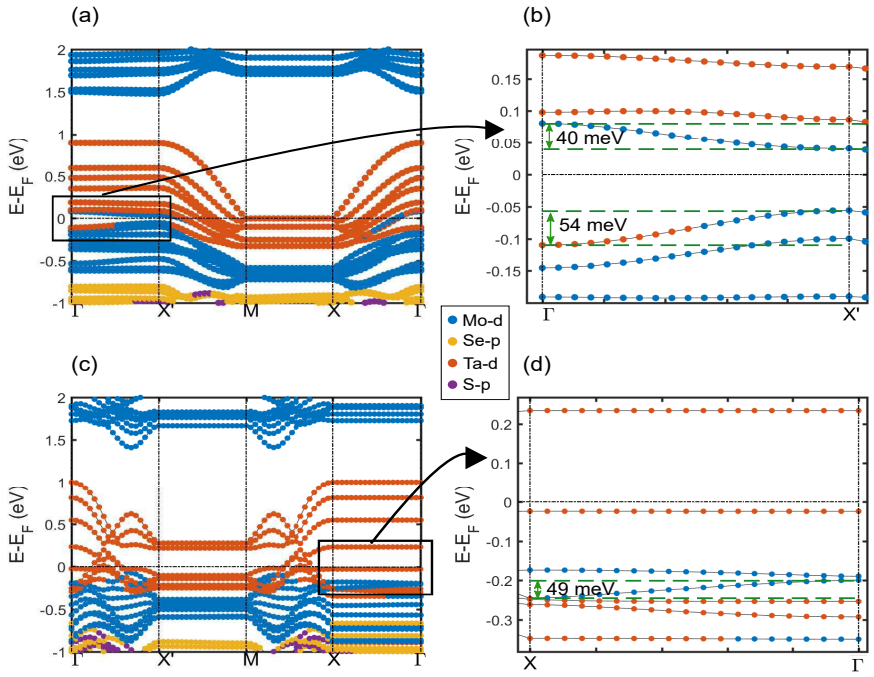

Figure 5.1: Band structure of $MoSe_2$-TaS_2 (a) armchair configuration (b) zoomed $\Gamma - X'$ area of k-path, (c) zigzag configuration and (d) zoomed $X - \Gamma$ area of k-path

heterostructure increasing length of the semiconducting region until the miniband width is a small fraction of the valence band offset. Once the miniband width is a small fraction of the band offset, we can rule out mini-band foemation as the source of the negative Schottky barrier.

Bibliography

[1] Cheng Gong, Hengji Zhang, Weihua Wang, Luigi Colombo, Robert M. Wallace, and Kyeongjae Cho. Band alignment of two-dimensional transition metal dichalcogenides: Application in tunnel field effect transistors. *Applied Physics Letters*, 103(5), 2013.

[2] Mingda Li, David Esseni, Gregory Snider, Debdeep Jena, and Huili Grace Xing. Single particle transport in two-dimensional heterojunction interlayer tunneling field effect transistor. *Journal of Applied Physics*, 115(7):074508, 2014.

[3] H. Ilatikhameneh, Y. Tan, B. Novakovic, G. Klimeck, R. Rahman, and J. Appenzeller. Tunnel field-effect transistors in 2-d transition metal dichalcogenide materials. *IEEE Journal on Exploratory Solid-State Computational Devices and Circuits*, 1:12–18, Dec 2015.

[4] M. O. Li, D. Esseni, J. J. Nahas, D. Jena, and H. G. Xing. Two-dimensional heterojunction interlayer tunneling field effect transistors (thin-tfets). *IEEE Journal of the Electron Devices Society*, 3(3):200–207, May 2015.

[5] Tania Roy, Mahmut Tosun, Xi Cao, Hui Fang, Der-Hsien Lien, Peida Zhao, Yu-Ze Chen, Yu-Lun Chueh, Jing Guo, and Ali Javey. Dual-gated mos2/wse2 van der waals tunnel diodes and transistors. *Acs Nano*, 9(2):2071–2079, 2015.

[6] Hesameddin Ilatikhameneh, Rajib Rahman, Joerg Appenzeller, and Gerhard Klimeck. Electrically doped wte 2 tunnel transistors. In *Simulation of Semiconductor Processes and Devices (SISPAD), 2015 International Conference on*, pages 270–272. IEEE, 2015.

[7] Oriol Lopez-Sanchez, Dominik Lembke, Metin Kayci, Aleksandra Radenovic, and Andras Kis. Ultrasensitive photodetectors based on monolayer mos2. *Nature nanotechnology*, 8(7):497–501, 2013.

[8] FHL Koppens, T Mueller, Ph Avouris, AC Ferrari, MS Vitiello, and M Polini. Photodetectors based on graphene, other two-dimensional materials and hybrid systems. *Nature nanotechnology*, 9(10):780–793, 2014.

[9] Dong-Ho Kang, Myung-Soo Kim, Jaewoo Shim, Jeaho Jeon, Hyung-Youl Park, Woo-Shik Jung, Hyun-Yong Yu, Chang-Hyun Pang, Sungjoo Lee, and Jin-Hong Park. High-performance transition metal dichalcogenide photodetectors enhanced by self-assembled monolayer doping. *Advanced Functional Materials*, 25(27):4219–4227, 2015.

[10] Zhaoqiang Zheng, Tanmei Zhang, Jiandomg Yao, Yi Zhang, Jiarui Xu, and Guowei Yang. Flexible, transparent and ultra-broadband photodetector based on large-area wse2 film for wearable devices. *Nanotechnology*, 27(22):225501, 2016.

[11] JD Yao, ZQ Zheng, JM Shao, and GW Yang. Stable, highly-responsive and broadband photodetection based on large-area multilayered ws 2 films grown by pulsed-laser deposition. *Nanoscale*, 7(36):14974–14981, 2015.

[12] Kin Fai Mak and Jie Shan. Photonics and optoelectronics of 2d semiconductor transition metal dichalcogenides. *Nature Photonics*, 10(4):216–226, 2016.

[13] Branimir Radisavljevic, Aleksandra Radenovic, Jacopo Brivio, i V Giacometti, and A Kis. Single-layer mos2 transistors. *Nature nanotechnology*, 6(3):147–150, 2011.

[14] Youngki Yoon, Kartik Ganapathi, and Sayeef Salahuddin. How good can monolayer mos2 transistors be? *Nano letters*, 11(9):3768–3773, 2011.

[15] Jiahao Kang, Wei Liu, and Kaustav Banerjee. High-performance mos2 transistors with low-resistance molybdenum contacts. *Applied Physics Letters*, 104(9):093106, 2014.

[16] Khairul Alam and Roger K Lake. Monolayer *mos* transistors beyond the technology road map. *IEEE transactions on electron devices*, 59(12):3250–3254, 2012.

[17] Somaia Sarwat Sylvia, Khairul Alam, and Roger K Lake. Uniform benchmarking of low-voltage van der waals fets. *IEEE Journal on Exploratory Solid-State Computational Devices and Circuits*, 2:28–35, 2016.

[18] Stefano Larentis, Babak Fallahazad, and Emanuel Tutuc. Field-effect transistors and intrinsic mobility in ultra-thin mose2 layers. *Applied Physics Letters*, 101(22), 2012.

[19] V Podzorov, ME Gershenson, Ch Kloc, R Zeis, and E Bucher. High-mobility field-effect transistors based on transition metal dichalcogenides. *Applied Physics Letters*, 84(17):3301–3303, 2004.

[20] V. Podzorov, M. E. Gershenson, Ch. Kloc, R. Zeis, and E. Bucher. High-mobility field-effect transistors based on transition metal dichalcogenides. *Applied Physics Letters*, 84(17):3301–3303, 2004.

[21] Hui Fang, Steven Chuang, Ting Chia Chang, Kuniharu Takei, Toshitake Takahashi, and Ali Javey. High-performance single layered wse2 p-fets with chemically doped contacts. *Nano Letters*, 12(7):3788–3792, 2012. PMID: 22697053.

[22] Saptarshi Das and Joerg Appenzeller. Wse2 field effect transistors with enhanced ambipolar characteristics. *Applied physics letters*, 103(10):103501, 2013.

[23] Saptarshi Das, Hong-Yan Chen, Ashish Verma Penumatcha, and Joerg Appenzeller. High performance multilayer mos2 transistors with scandium contacts. *Nano letters*, 13(1):100–105, 2012.

[24] Hai Li, Zongyou Yin, Qiyuan He, Hong Li, Xiao Huang, Gang Lu, Derrick Wen Hui Fam, Alfred Iing Yoong Tok, Qing Zhang, and Hua Zhang. Fabrication of single- and multilayer mos2 film-based field-effect transistors for sensing no at room temperature. *small*, 8(1):63–67, 2012.

[25] Adam L Friedman, F Keith Perkins, Enrique Cobas, Glenn G Jernigan, Paul M Campbell, Aubrey T Hanbicki, and Berend T Jonker. Chemical vapor sensing of two-dimensional mos 2 field effect transistor devices. *Solid-State Electronics*, 101:2–7, 2014.

[26] Hsun-Jen Chuang, Bhim Chamlagain, Michael Koehler, Meeghage Madusanka Perera, Jiaqiang Yan, David Mandrus, David Tomanek, and Zhixian Zhou. Low-resistance 2d/2d ohmic contacts: A universal approach to high-performance wse2, mos2, and mose2 transistors. *Nano letters*, 16(3):1896–1902, 2016.

[27] Adam L Friedman, F Keith Perkins, Aubrey T Hanbicki, James C Culbertson, and Paul M Campbell. Dynamics of chemical vapor sensing with mos 2 using 1t/2h phase contacts/channel. *Nanoscale*, 8(22):11445–11453, 2016.

[28] Manish Chhowalla, Hyeon Suk Shin, Goki Eda, Lain-Jong Li, Kian Ping Loh, and Hua Zhang. The chemistry of two-dimensional layered transition metal dichalcogenide nanosheets. *Nature chemistry*, 5(4):263–275, 2013.

[29] Han Liu, Adam T Neal, and Peide D Ye. Channel length scaling of mos2 mosfets. *ACS nano*, 6(10):8563–8569, 2012.

[30] Yu Chai, Robert Ionescu, Shanshan Su, Roger Lake, Mihrimah Ozkan, and Cengiz S Ozkan. Making one-dimensional electrical contacts to molybdenum disulfide-based heterostructures through plasma etching. *physica status solidi (a)*, 213(5):1358–1364, 2016.

[31] Yu Chai, Shanshan Su, Dong Yan, Mihrimah Ozkan, Roger Lake, and Cengiz S Ozkan. Strain gated bilayer molybdenum disulfide field effect transistor with edge contacts. *Scientific Reports*, 7:41593, 2017.

[32] Pradyumna Goli, Javed Khan, Darshana Wickramaratne, Roger K Lake, and Alexander A Balandin. Charge density waves in exfoliated films of van der waals materials: evolution of raman spectrum in tise2. *Nano letters*, 12(11):5941–5945, 2012.

[33] J Khan, CM Nolen, D Teweldebrhan, D Wickramaratne, RK Lake, and AA Balandin. Anomalous electron transport in back-gated field-effect transistors with tite2 semimetal thin-film channels. *Applied Physics Letters*, 100(4):043109, 2012.

[34] Rohan Dhall, Mahesh R Neupane, Darshana Wickramaratne, Matthew Mecklenburg, Zhen Li, Cameron Moore, Roger K Lake, and Stephen Cronin. Direct bandgap transition in many-layer mos2 by plasma-induced layer decoupling. *Advanced Materials*, 27(9):1573–1578, 2015.

[35] R Samnakay, D Wickramaratne, TR Pope, RK Lake, TT Salguero, and AA Balandin. Zone-folded phonons and the commensurate–incommensurate charge-density-wave transition in 1 t-tase2 thin films. *Nano letters*, 15(5):2965–2973, 2015.

[36] J Renteria, R Samnakay, C Jiang, TR Pope, P Goli, Z Yan, D Wickramaratne, TT Salguero, AG Khitun, RK Lake, et al. All-metallic electrically gated 2h-tase2 thin-film switches and logic circuits. *Journal of Applied Physics*, 115(3):034305, 2014.

[37] Gianluca Fiori, Francesco Bonaccorso, Giuseppe Iannaccone, Tomás Palacios, Daniel Neumaier, Alan Seabaugh, Sanjay K Banerjee, and Luigi Colombo. Electronics based on two-dimensional materials. *Nature nanotechnology*, 9(10):768–779, 2014.

[38] Darshana Wickramaratne, Ferdows Zahid, and Roger K Lake. Electronic and thermoelectric properties of few-layer transition metal dichalcogenides. *The Journal of chemical physics*, 140(12):124710, 2014.

[39] Darshana Wickramaratne, Ferdows Zahid, and Roger K Lake. Electronic and thermoelectric properties of van der waals materials with ring-shaped valence bands. *Journal of Applied Physics*, 118(7):075101, 2015.

[40] Shanshan Su, Protik Das, Supeng Ge, and Roger K Lake. Graphene contacts to a hfse2/sns2 heterostructure. *The Journal of Chemical Physics*, 146(6):064701, 2017.

[41] Cheng Gong, Luigi Colombo, Robert M Wallace, and Kyeongjae Cho. The unusual mechanism of partial fermi level pinning at metal–mos2 interfaces. *Nano letters*, 14(4):1714–1720, 2014.

[42] Neelam Kaushik, Ankur Nipane, Firdous Basheer, Souvik Dubey, Sachit Grover, Minal Deshmukh, and Saurabh Lodha. Evaluating au and pd contacts in mono and multilayer mos 2 transistors. In *Device Research Conference (DRC), 2014 72nd Annual*, pages 195–196. IEEE, 2014.

[43] Kuan Zhou, Darshana Wickramaratne, Supeng Ge, Shanshan Su, Amrit De, and Roger K Lake. Interlayer resistance of misoriented mos 2. *Physical Chemistry Chemical Physics*, 19(16):10406–10412, 2017.

[44] Raymond T Tung. Formation of an electric dipole at metal-semiconductor interfaces. *Physical review B*, 64(20):205310, 2001.

[45] Volker Heine. Theory of surface states. *Physical Review*, 138(6A):A1689, 1965.

[46] J Tersoff. Schottky barrier heights and the continuum of gap states. *Physical Review Letters*, 52(6):465, 1984.

[47] Rajesh Kappera, Damien Voiry, Sibel Ebru Yalcin, Brittany Branch, Gautam Gupta, Aditya D Mohite, and Manish Chhowalla. Phase-engineered low-resistance contacts for ultrathin mos2 transistors. *Nature materials*, 13(12):1128–1134, 2014.

[48] Yuanyue Liu, Paul Stradins, and Su-Huai Wei. Van der waals metal-semiconductor junction: Weak fermi level pinning enables effective tuning of schottky barrier. *Science advances*, 2(4):e1600069, 2016.

[49] Jiahao Kang, Wei Liu, Deblina Sarkar, Debdeep Jena, and Kaustav Banerjee. Computational study of metal contacts to monolayer transition-metal dichalcogenide semiconductors. *Physical Review X*, 4(3):031005, 2014.

[50] http://www.itrs2.net/.

[51] Alan Allan, Don Edenfeld, William H Joyner, Andrew B Kahng, Mike Rodgers, and Yervant Zorian. 2001 technology roadmap for semiconductors. *Computer*, 35(1):42–53, 2002.

[52] Wolfgang M Arden. The international technology roadmap for semiconductorsperspectives and challenges for the next 15 years. *Current Opinion in Solid State and Materials Science*, 6(5):371–377, 2002.

[53] Deep Jariwala, Vinod K. Sangwan, Lincoln J. Lauhon, Tobin J. Marks, and Mark C. Hersam. Carbon nanomaterials for electronics, optoelectronics, photovoltaics, and sensing. *Chem. Soc. Rev.*, 42:2824–2860, 2013.

[54] A. H. Castro Neto, F. Guinea, N. M. R. Peres, K. S. Novoselov, and A. K. Geim. The electronic properties of graphene. *Rev. Mod. Phys.*, 81:109–162, Jan 2009.

[55] Valeria Nicolosi, Manish Chhowalla, Mercouri G Kanatzidis, Michael S Strano, and Jonathan N Coleman. Liquid exfoliation of layered materials. *Science*, 340(6139):1226419, 2013.

[56] Qing Hua Wang, Kourosh Kalantar-Zadeh, Andras Kis, Jonathan N Coleman, and Michael S Strano. Electronics and optoelectronics of two-dimensional transition metal dichalcogenides. *Nature nanotechnology*, 7(11):699–712, 2012.

[57] Sheneve Z Butler, Shawna M Hollen, Linyou Cao, Yi Cui, Jay A Gupta, Humberto R Gutierrez, Tony F Heinz, Seung Sae Hong, Jiaxing Huang, Ariel F Ismach, et al. Progress, challenges, and opportunities in two-dimensional materials beyond graphene. *ACS nano*, 7(4):2898–2926, 2013.

[58] AK Geim and IV Grigorieva. Van der waals heterostructures. *Nature*, 499(7459):419–425, 2013.

[59] Xiao Huang, Zhiyuan Zeng, and Hua Zhang. Metal dichalcogenide nanosheets: preparation, properties and applications. *Chemical Society Reviews*, 42(5):1934–1946, 2013.

[60] J. A. Wilson and A. D. Yoffe. The transition metal dichalcogenides discussion and interpretation of the observed optical, electrical and structural properties. *Advances in Physics*, 18:193–335, 1969.

[61] LF Mattheiss. Band structures of transition-metal-dichalcogenide layer compounds. *Physical Review B*, 8(8):3719, 1973.

[62] AM Woolley and G Wexler. Band structures and fermi surfaces for 1t-tas2, 1t-tase2 and 1t-vse2. *Journal of Physics C: Solid State Physics*, 10(14):2601, 1977.

[63] Jl A Wilson, FJ Di Salvo, and S Mahajan. Charge-density waves and superlattices in the metallic layered transition metal dichalcogenides. *Advances in Physics*, 24(2):117–201, 1975.

[64] Tatsuya Shishidou, AJ Freeman, and Ryoji Asahi. Effect of gga on the half-metallicity of the itinerant ferromagnet cos 2. *Physical Review B*, 64(18):180401, 2001.

[65] R Fivaz and E Mooser. Electron-phonon interaction in semiconducting layer structures. *Physical Review*, 136(3A):A833, 1964.

[66] R_ Fivaz and E Mooser. Mobility of charge carriers in semiconducting layer structures. *Physical Review*, 163(3):743, 1967.

[67] JT Ye, YJ Zhang, R Akashi, MS Bahramy, R Arita, and Y Iwasa. Superconducting dome in a gate-tuned band insulator. *Science*, 338(6111):1193–1196, 2012.

[68] JA Wilson, FJ Di Salvo, and S Mahajan. Charge-density waves in metallic, layered, transition-metal dichalcogenides. *Physical review letters*, 32(16):882, 1974.

[69] WL McMillan. Landau theory of charge-density waves in transition-metal dichalcogenides. *Physical Review B*, 12(4):1187, 1975.

[70] AH Castro Neto. Charge density wave, superconductivity, and anomalous metallic behavior in 2d transition metal dichalcogenides. *Physical review letters*, 86(19):4382, 2001.

[71] RL Withers and JA Wilson. An examination of the formation and characteristics of charge-density waves in inorganic materials with special reference to the two- and one-dimensional transition-metal chalcogenides. *Journal of physics. C. Solid state physics*, 19(25):4809–4845, 1986.

[72] JA Wilson and AD Yoffe. The transition metal dichalcogenides discussion and interpretation of the observed optical, electrical and structural properties. *Advances in Physics*, 18(73):193–335, 1969.

[73] AD Yoffe. Layer compounds. *Annual Review of Materials Science*, 3(1):147–170, 1973.

[74] Graeme Cunningham, Mustafa Lotya, Clotilde S Cucinotta, Stefano Sanvito, Shane D Bergin, Robert Menzel, Milo SP Shaffer, and Jonathan N Coleman. Solvent exfoliation of transition metal dichalcogenides: dispersibility of exfoliated nanosheets varies only weakly between compounds. *ACS nano*, 6(4):3468–3480, 2012.

[75] Ruitao Lv, Joshua A Robinson, Raymond E Schaak, Du Sun, Yifan Sun, Thomas E Mallouk, and Mauricio Terrones. Transition metal dichalcogenides and beyond: synthesis, properties, and applications of single-and few-layer nanosheets. *Accounts of chemical research*, 48(1):56–64, 2014.

[76] Yi-Hsien Lee, Xin-Quan Zhang, Wenjing Zhang, Mu-Tung Chang, Cheng-Te Lin, Kai-Di Chang, Ya-Chu Yu, Jacob Tse-Wei Wang, Chia-Seng Chang, Lain-Jong Li, et al. Synthesis of large-area mos2 atomic layers with chemical vapor deposition. *Advanced Materials*, 24(17):2320–2325, 2012.

[77] Jonathan N Coleman, Mustafa Lotya, Arlene ONeill, Shane D Bergin, Paul J King, Umar Khan, Karen Young, Alexandre Gaucher, Sukanta De, Ronan J Smith, et al. Two-dimensional nanosheets produced by liquid exfoliation of layered materials. *Science*, 331(6017):568–571, 2011.

[78] Atsushi Koma. Van der waals epitaxya new epitaxial growth method for a highly lattice-mismatched system. *Thin Solid Films*, 216(1):72–76, 1992.

[79] Yazeed Alaskar, Shamsul Arafin, Darshana Wickramaratne, Mark A Zurbuchen, Liang He, Jeff McKay, Qiyin Lin, Mark S Goorsky, Roger K Lake, and Kang L Wang. Towards van der waals epitaxial growth of gaas on si using a graphene buffer layer. *Advanced Functional Materials*, 24(42):6629–6638, 2014.

[80] Raymond T Tung and . The physics and chemistry of the schottky barrier height. *Applied Physics Reviews*, 1(1):011304, 2014.

[81] Simon M Sze and Kwok K Ng. *Physics of semiconductor devices*. John wiley & sons, 2006.

[82] HH Berger. Contact resistance and contact resistivity. *Journal of the Electrochemical Society*, 119(4):507–514, 1972.

[83] Daria Krasnozhon, Dominik Lembke, Clemens Nyffeler, Yusuf Leblebici, and Andras Kis. Mos2 transistors operating at gigahertz frequencies. *Nano letters*, 14(10):5905–5911, 2014.

[84] Changsik Kim, Inyong Moon, Daeyeong Lee, Min Sup Choi, Faisal Ahmed, Seunggeol Nam, Yeonchoo Cho, Hyeon-Jin Shin, Seongjun Park, and Won Jong Yoo. Fermi level pinning at electrical metal contacts of monolayer molybdenum dichalcogenides. *ACS nano*, 11(2):1588–1596, 2017.

[85] Hui Fang, Steven Chuang, Ting Chia Chang, Kuniharu Takei, Toshitake Takahashi, and Ali Javey. High-performance single layered wse2 p-fets with chemically doped contacts. *Nano letters*, 12(7):3788–3792, 2012.

[86] Hui Yuan, Guangjun Cheng, Lin You, Haitao Li, Hao Zhu, Wei Li, Joseph J Kopanski, Yaw S Obeng, Angela R Hight Walker, David J Gundlach, et al. Influence of metal–mos2 interface on mos2 transistor performance: Comparison of ag and ti contacts. *ACS applied materials & interfaces*, 7(2):1180–1187, 2015.

[87] Ah Ra Kim, Yonghun Kim, Jaewook Nam, Hee-Suk Chung, Dong Jae Kim, Jung-Dae Kwon, Sang Won Park, Jucheol Park, Sun Young Choi, Byoung Hun Lee, et al. Alloyed 2d metal–semiconductor atomic layer junctions. *Nano letters*, 16(3):1890–1895, 2016.

[88] Jie Guan, Hsun-Jen Chuang, Zhixian Zhou, and David Tomanek. Optimizing charge injection across transition metal dichalcogenide heterojunctions: Theory and experiment. *ACS nano*, 11(4):3904–3910, 2017.

[89] Yohta Sata, Rai Moriya, Satoru Masubuchi, Kenji Watanabe, Takashi Taniguchi, and Tomoki Machida. N-and p-type carrier injections into wse2 with van der waals contacts of two-dimensional materials. *Japanese Journal of Applied Physics*, 56(4S):04CK09, 2017.

[90] Dimitra Tsoutsou, Kleopatra E Aretouli, Polychronis Tsipas, Jose Marquez-Velasco, Evangelia Xenogiannopoulou, Nikolaos Kelaidis, Sigiava Aminalragia Giamini, and Athanasios Dimoulas. Epitaxial 2d mose2 (hfse2) semiconductor/2d tase2 metal van der waals heterostructures. *ACS applied materials & interfaces*, 8(3):1836–1841, 2016.

[91] Stephen McDonnell, Angelica Azcatl, Rafik Addou, Cheng Gong, Corsin Battaglia, Steven Chuang, Kyeongjae Cho, Ali Javey, and Robert M Wallace. Hole contacts on transition metal dichalcogenides: Interface chemistry and band alignments. *ACS nano*, 8(6):6265–6272, 2014.

[92] Lili Yu, Yi-Hsien Lee, Xi Ling, Elton JG Santos, Yong Cheol Shin, Yuxuan Lin, Madan Dubey, Efthimios Kaxiras, Jing Kong, Han Wang, et al. Graphene/mos2 hybrid technology for large-scale two-dimensional electronics. *Nano letters*, 14(6):3055–3063, 2014.

[93] Willian Couto, Adalberto Fazzio, and Roberto Miwa. Tuning the p-type schottky barrier in 2d metal/semiconductor interface: boron-sheet/\mose, and/\wse. *arXiv preprint arXiv:1702.00437*, 2017.

[94] Suyeon Cho, Sera Kim, Jung Ho Kim, Jiong Zhao, Jinbong Seok, Dong Hoon Keum, Jaeyoon Baik, Duk-Hyun Choe, KJ Chang, Kazu Suenaga, et al. Phase patterning for ohmic homojunction contact in mote2. *Science*, 349(6248):625–628, 2015.

[95] G Wexler and AM Woolley. Fermi surfaces and band structures of the 2h metallic transition-metal dichalcogenides. *Journal of Physics C: Solid State Physics*, 9(7):1185, 1976.

[96] Anthony Ayari, Enrique Cobas, Ololade Ogundadegbe, and Michael S Fuhrer. Realization and electrical characterization of ultrathin crystals of layered transition-metal dichalcogenides. *Journal of applied physics*, 101(1):14507–14507, 2007.

[97] Yi Ding, Yanli Wang, Jun Ni, Lin Shi, Siqi Shi, and Weihua Tang. First principles study of structural, vibrational and electronic properties of graphene-like mx 2 (m= mo, nb, w, ta; x= s, se, te) monolayers. *Physica B: Condensed Matter*, 406(11):2254–2260, 2011.

[98] Young-Jun Yu, Yue Zhao, Sunmin Ryu, Louis E Brus, Kwang S Kim, and Philip Kim. Tuning the graphene work function by electric field effect. *Nano letters*, 9(10):3430–3434, 2009.

[99] Chih-Jen Shih, Qing Hua Wang, Youngwoo Son, Zhong Jin, Daniel Blankschtein, and Michael S Strano. Tuning on–off current ratio and field-effect mobility in a mos2–graphene heterostructure via schottky barrier modulation. *ACS nano*, 8(6):5790–5798, 2014.

[100] He Tian, Zhen Tan, Can Wu, Xiaomu Wang, Mohammad Ali Mohammad, Dan Xie, Yi Yang, Jing Wang, Lain-Jong Li, Jun Xu, et al. Novel field-effect schottky barrier transistors based on graphene-mos2 heterojunctions. *Scientific reports*, 4:5951, 2014.

[101] Yuan Liu, Hao Wu, Hung-Chieh Cheng, Sen Yang, Enbo Zhu, Qiyuan He, Mengning Ding, Dehui Li, Jian Guo, Nathan O Weiss, et al. Toward barrier free contact to molybdenum disulfide using graphene electrodes. *Nano letters*, 15(5):3030–3034, 2015.

[102] Pierre Hohenberg and Walter Kohn. Inhomogeneous electron gas. *Physical review*, 136(3B):B864, 1964.

[103] W. Kohn and L. J. Sham. Self-consistent equations including exchange and correlation effects. *Phys. Rev.*, 140:A1133–A1138, Nov 1965.

[104] John P Perdew, Kieron Burke, and Matthias Ernzerhof. Generalized gradient approximation made simple. *Physical review letters*, 77(18):3865, 1996.

[105] Matthias Ernzerhof and Gustavo E Scuseria. Assessment of the perdew–burke–ernzerhof exchange-correlation functional. *The Journal of chemical physics*, 110(11):5029–5036, 1999.

[106] Georg Kresse and Jürgen Furthmüller. Efficiency of ab-initio total energy calculations for metals and semiconductors using a plane-wave basis set. *Computational Materials Science*, 6(1):15–50, 1996.

[107] Yan Li, Sefaattin Tongay, Qu Yue, Jun Kang, Junqiao Wu, and Jingbo Li. Metal to semiconductor transition in metallic transition metal dichalcogenides. *Journal of Applied Physics*, 114(17):174307, 2013.

[108] Agnieszka Kuc, Nourdine Zibouche, and Thomas Heine. Influence of quantum confinement on the electronic structure of the transition metal sulfide t s 2. *Physical Review B*, 83(24):245213, 2011.

[109] Ashok Kumar and PK Ahluwalia. Effect of quantum confinement on electronic and dielectric properties of niobium dichalcogenides nbx 2 (x= s, se, te). *Journal of Alloys and Compounds*, 550:283–291, 2013.

[110] Priya Johari and Vivek B Shenoy. Tunable dielectric properties of transition metal dichalcogenides. *ACS nano*, 5(7):5903–5908, 2011.

[111] Can Ataca, Hasan Sahin, and Salim Ciraci. Stable, single-layer mx2 transition-metal oxides and dichalcogenides in a honeycomb-like structure. *The Journal of Physical Chemistry C*, 116(16):8983–8999, 2012.

[112] Stefan Grimme, Jens Antony, Stephan Ehrlich, and Helge Krieg. A consistent and accurate ab initio parametrization of density functional dispersion correction (dft-d) for the 94 elements h-pu. *The Journal of chemical physics*, 132(15):154104, 2010.

[113] Yongji Gong, Junhao Lin, Xingli Wang, Gang Shi, Sidong Lei, Zhong Lin, Xiaolong Zou, Gonglan Ye, Robert Vajtai, Boris I Yakobson, et al. Vertical and in-plane heterostructures from ws2/mos2 monolayers. *Nature materials*, 13(12):1135–1142, 2014.

[114] Ming-Yang Li, Yumeng Shi, Chia-Chin Cheng, Li-Syuan Lu, Yung-Chang Lin, Hao-Lin Tang, Meng-Lin Tsai, Chih-Wei Chu, Kung-Hwa Wei, Jr-Hau He, et al. Epitaxial growth of a monolayer wse2-mos2 lateral pn junction with an atomically sharp interface. *Science*, 349(6247):524–528, 2015.

[115] AR Botello-Mendez, F Lopez-Urias, M Terrones, and H Terrones. Metallic and ferromagnetic edges in molybdenum disulfide nanoribbons. *Nanotechnology*, 20(32):325703, 2009.